

Corrosion behavior of nano bio coating on AZ31 magnesium alloy by electrophoretic deposition for biomedical application

Maream Ali Radhi¹, Ali Mundher Mustafa^{1*} , Makarim H. Abdulkareem¹

¹ College of Production Engineering and Metallurgy, University of Technology, Baghdad, Iraq

* Corresponding author's e-mail: Ali.m.mustafa@uotechnology.edu.iq

ABSTRACT

Magnesium alloy AZ31 is a promising material for biodegradable implants due to its mechanical similarity to bone and its natural degradation in the body, eliminating the need for surgical removal. However, its clinical application is limited by rapid corrosion and susceptibility to bacterial colonization. This study addresses these challenges by applying nano-scale bioactive coatings of hydroxyapatite (HA) and calcium oxide (CaO) onto AZ31 using electrophoretic deposition (EPD). Coatings were deposited under optimized conditions (20 V, 4 minutes, 5 wt%) and evaluated for morphology, thickness, wettability, antibacterial activity, and bioactivity. Single and multilayer coatings showed thicknesses from 21.23 μm to over 100 μm . SEM and EDS analyses confirmed uniform, crack-free coatings with strong adhesion. Zeta potential measurements above +30 mV indicated stable suspensions, while contact angle measurements revealed significantly enhanced hydrophilicity, especially in triple-layer coatings, which showed a contact angle as low as 1.58°. Antibacterial assays demonstrated strong inhibition of *Staphylococcus aureus*, with inhibition zones up to 46 mm, while the uncoated alloy showed no antibacterial effect. After 14 days in simulated body fluid, all coated samples exhibited apatite formation, indicating improved bioactivity. The best performance was observed in the triple-layer configuration (CaO + (HA+CaO) + HA), which achieved the lowest corrosion current density (0.0619633 μA) and the highest corrosion potential (-895.349 mV). These results indicate that this multilayer coating forms an effective protective barrier against corrosion and enhances the biological performance of AZ31. Overall, nano HA/CaO multilayer coatings significantly improve the corrosion resistance, antibacterial properties, and bioactivity of AZ31, supporting their potential use in biodegradable implant applications.

Keywords: corrosion resistance, AZ31 magnesium alloy, electrophoretic deposition, hydroxyapatite, calcium oxide.

INTRODUCTION

Biomaterials are designed to interact with living tissues to replace, repair, or restore biological functions. Their effective integration with the body is made possible by a range of mechanical, biological, chemical, and physical properties that support safe and functional use within or on the human body [1–2]. Biomedical materials can be classified based on various factors, including their inherent properties, behavior within the body, and long-term biocompatibility. They are commonly divided into three main categories: metal biomaterials, ceramic biomaterials, and polymer biomaterials each offering distinct characteristics

such as antibacterial activity and bioactivity. These materials play essential roles across all medical disciplines. They are used in diverse applications such as drug delivery systems, tissue scaffolds, prosthetic organs or components, and various types of implants [3–5].

Materials (metals, ceramics, polymers and their composites) must be carefully chosen and manufactured to combine biocompatibility with particular qualities based on the device's intended purpose, such as density, elasticity, resistance to fracture and wear, etc., in order to be utilized as implants. Due to their exceptional strength and ductility, metals have traditionally been the most popular material for implants. In

particular, stainless steel, Ti alloys, and CoCr alloys are often used due to their high corrosion resistance [6–8]. However, the release of ions from the metallic surface, the chemical reaction of a metallic surface with the body's enzymes and acids, toxicity, galvanic or oxidative corrosion, and stress shielding (bone resorption) can all result in implant failure. This can lead to a decrease in the vascularity of surrounding tissue [9–10]. Therefore, in order to get around these drawbacks of traditional metallic implants, researchers and physicians have turned their focus to biodegradable materials. As a result, a biodegradable implant material that remains intact for a period of time to allow damaged tissue in the human body to recuperate before gradually dissolving, absorbing, excreting, or consuming, so avoiding a second surgery, is an appealing concept [11–13].

Biodegradable magnesium (Mg) has steadily gathered a lot of interest in the biomedical field. In addition to having a density of 1.74 g/cm³ and an elastic modulus of 41–45 GPa, which are comparable to those of human bone, it also has good biocompatibility. Magnesium is a necessary nutrient for human health since it can help osteoblasts differentiate and biomineralize, improve cell adherence to biomaterials, and encourage bone formation [14–17]. However, Mg and its alloys have severe degradation reactions in the physiological environment, resulting in the quick evolution of hydrogen gas and loss of mechanical integrity before complete healing, resulting in impaired bone healing and failure of internal fixation [18–20]. In addition, bacteria might adhere and colonize on the surface of implants during tissue repair, which would rapidly proliferate and form eventually a dense bacterial film to greatly inhibit the killing effect of antibiotics and block subsequent osteogenesis, and thus leading to implant failure. Hence, developing multifunctional Mg-based implants with good corrosion resistance, antibacterial ability and osteogenic activity is highly desirable to meet complex clinical needs [20–21].

Surface modification techniques aim to enhance the biocompatibility of metallic implants by altering their surface properties without affecting the bulk material's mechanical integrity. One of the most common goals of surface modification is to reduce the risk of infection and improve the healing process by creating a surface that is more conducive to tissue growth and repair. The future of surface modification for metallic implants lies

in the development of multifunctional coatings that not only enhance biocompatibility but also provide antimicrobial properties, reducing the risk of infection. Several surface modification methods, including physical vapor deposition (PVD), chemical vapor deposition (CVD), ion implantation, and laser treatment, are employed to alter the surface characteristics of metallic implants. A range of coatings, such as bioactive ceramics, polymers, or even protein layers, can be introduced by these procedures, improving cell adhesion and encouraging advantageous biological reactions [23].

The structure of hydroxyapatite closely resembles that of natural bone, making it a preferred material for dental and orthopedic implants. This structural similarity allows hydroxyapatite (HAP) coatings to introduce beneficial surface properties such as osteointegration and biocompatibility, which significantly improve implant performance. To be effective, HAP coatings must not only exhibit suitable mechanical properties, high bonding strength, and corrosion resistance, but also maintain compatibility with surrounding biological tissues. [24]. Bone is a complex natural composition made up of both inorganic and organic materials. Combining the two elements' results in reinforced materials, wherein inorganic ingredients give the material strength and organic materials give it flexibility [25].

A naturally occurring organic substance made from chitin, chitosan is well-known for its numerous biomedical uses and biocompatibility. Since its breakdown products are non-toxic, chitosan's hydrophilic surface encourages cell attachment and proliferation. Chitosan is especially appealing as a bone scaffold material due to its ability to promote osteoblast adhesion, proliferation, and *in vitro* bone formation. When combined with various materials such as polymers and ceramics, it can be used to create composite scaffolds with enhanced mechanical and biological properties. EPD is a widely used technique for coating these materials, valued for its versatility and efficiency. EPD allows the deposition of dense, high-purity coatings on complex-shaped substrates at room temperature, offering a rapid, cost-effective, and scalable solution. [26–28]. To enhance the corrosion resistance, antibacterial properties, and bioactivity of biodegradable magnesium-based implants, this study aims to develop a multifunctional coating. Specifically, the research focuses on improving implant longevity, minimizing

bacterial adhesion, and promoting osteointegration by applying hydroxyapatite (HA) and calcium oxide (CaO) coatings to AZ31 magnesium alloy using EPD [29–30].

EXPERIMENTAL PROCEDURE

Suspension and substrate preparation

The chemical composition analysis of the AZ31 substrate was conducted using an optical emission spectrometer (OES), with results shown in Table 1. Chitosan (medium molecular weight, 85% degree of deacetylation) was obtained from Sigma Aldrich and employed as a biopolymer in this investigation, as well as a binder for the ceramic material. Sigma Aldrich provided hydroxyapatite (a reagent grade synthetic powder with 30–100 nm particle size, 99% purity, white color, and 3.140 g/cm³ density) for the coating layer. Furthermore, Nano MgO (20–30 nm, 99.8% purity, white), Nano ZnO structured as 3% rods (20–30 nm, 99.8% purity, white), and Nano CaO (20–30 nm, 99.8% purity, white) were utilized in creating the coatings. The experimental methods involved the use of deionized water along with solvents, including absolute ethanol (99.9%) and acetic acid (99.5% purity). The surfaces were ground using silicon carbide (SiC) abrasive sheets with grit numbers of 240, 500, and 800, resulting in approximate surface roughness values of 1.053, 0.438, and 0.188 μm, as indicated in Table 2. After 15 minutes of ultrasonic cleaning in acetone, all samples were left to dry at room temperature prior to deposition. Three distinct compositions were used to prepare the solutions. HA is present in the first solution at a concentration of 3%. Five percent of calcium oxide (CaO) is included in the second one. The final one was a HA and CaO composite, containing 3% HA and 5% CaO. 0.5 g/L of chitosan, 1% acetic acid, 94% ethanol, and 5% deionized water were utilized in each solution. The suspensions were shaken for 24 hours prior to undergoing a 30-minute ultrasonic treatment in order to ensure sufficient dispersion. The pH of each solution

was regulated to 5. All samples were coated using the EPD process after the solution was prepared. The EPD cell utilized in this investigation was made up of two electrodes immersed in a suspension-filled beaker. Before testing, the anode and cathode were cleaned with acetone and dried, and the electrode spacing was fixed at 1 cm. During the deposition procedure, an electrode was placed in a 50 ml beaker filled with the prepared coating solution. The deposition process took place for four minutes at a voltage of twenty volts. A zeta potential test was performed to evaluate the stability of the suspensions. The surface layer was characterized using optical microscopy.

RESULTS AND DISCUSSION

Solution stability (zeta potential)

Zeta potential (ζ) is a key factor in EPD since it determines the stability of the suspension, ensures a homogeneous solution, and produces a uniform coating. The electrophoretic mobility and zeta potential values of the solutions employed for monolayer and multilayer deposition are shown in Table 3. Biomedical applications require optimal particle dispersion and deposition efficiency, which can only be achieved by comprehending zeta potential and electrophoretic mobility. All of the zeta potential measurements were positive since the pH was adjusted to 4. The suspension was stable and evenly distributed, as evidenced by the high absolute zeta potential values. These data illustrate the zeta potential measurements for HA 3%, CaO 5%, and the HA/CaO composite solutions. Furthermore, all suspensions were found to be appropriate for EPD

Table 2. Roughness values corresponding to smoothing papers

No.	Degree of grid of grinding paper	Roughness measurement (μm)
1	240	1.053
2	500	0.438
3	800	0.188

Table 1. Chemical composition for AZ31

Elements	Al	Zn	Mn	Fe	Cu	Ni	Si
ASTM Standard	2.4–3.6	0.5–1.5	0.2–1	0.003	< 0.05	< 0.005	< 0.1
Measurement	3.01	0.912	0.127	0.003	< 0.0020	0.0062	0.0498

Table 3. The value of mobility and zeta potential

Suspension type	Zeta potential (mv)	Mobility
HA	57	4.44
CaO	35	0.99
HA/CaO	49.71	2.73

since these values predicted cathodic deposition. As the absolute zeta potential values increased, electrophoretic mobility also increased. In order to stabilize the dispersion and improve particle interactions, chitosan binding agent utilized in the suspension was essential. Its existence raised the HA particles' surface charge, which raised their zeta potential and, as a result, improved their electrophoretic mobility. This improved the uniformity of the deposited layers and prevented

agglomeration by facilitating more effective particle movement. Greater mobility in the solution brought about by higher zeta potential values enhanced suspension stability and accelerated deposition rates, guaranteeing full substrate coverage. Since ethanol works well at dispersing substances like HA, it was chosen as the suspending medium. The findings verified that the composite particles in the EPD suspension were positively charged and deposited onto the cathode electrode since both chitosan and hydroxyapatite showed a positive zeta potential.

Microstructure analysis for final layers

The surface topography and coating thickness were examined using the optical microscope and scanning electron microscope (SEM), as shown

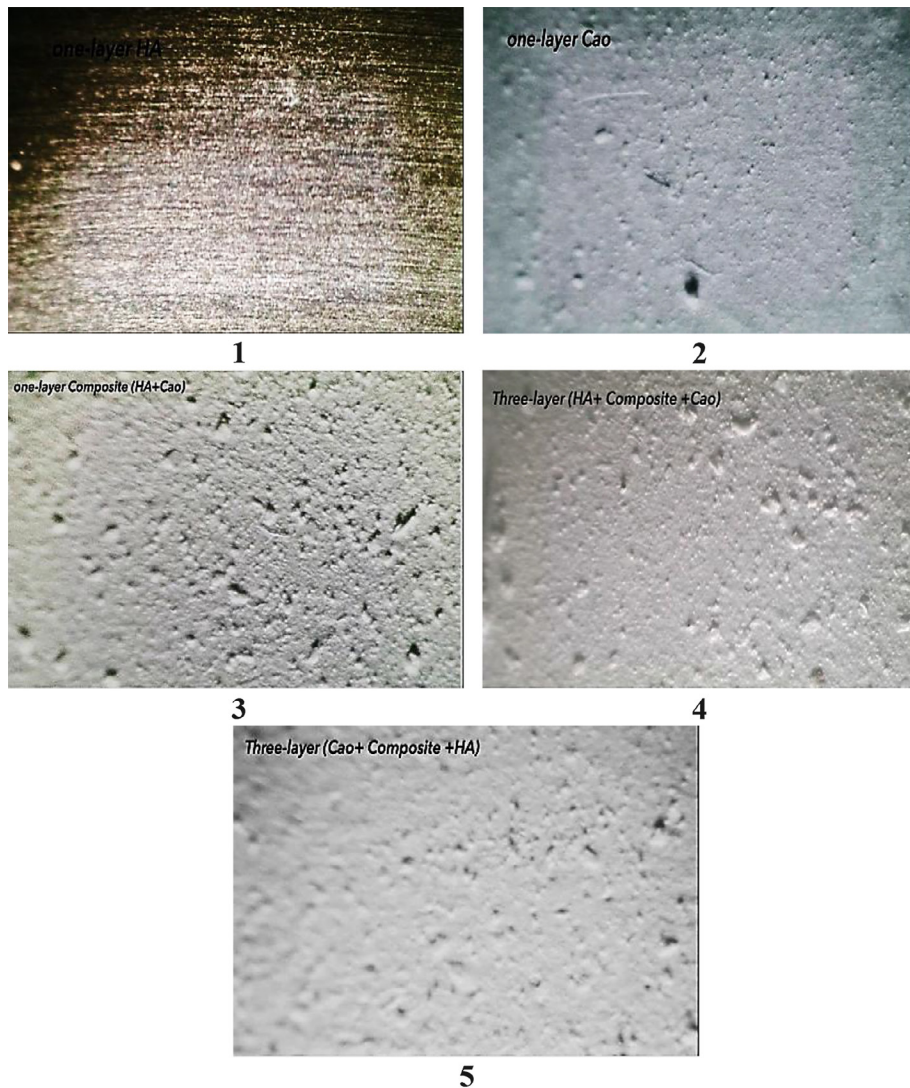


Figure 1. Optical images of topography for coating samples. (1) one-layer HA, (2) one-layer CaO, (3) one-layer Composite (HA+CaO), (4) Three-layer (HA+ Composite +CaO) and (5) Three-layer (CaO+ Composite +HA)

in Figure 1 (1) to (5). According to observations, the coating has a solid structure and is noticeably thick, both of which were attained under optimum deposition conditions. A concentration of 3% HA and 5% calcium oxide (CaO) was used for the deposition process, which was carried out at 20 V for four minutes. Based on the Taguchi design of experiments (DOE), these parameters were chosen. The thickness of the last layer of HA alone, as depicted in Figure 2 (1), was found to be roughly 21.231 μm . The CaO layer, on the other hand, has a consistent and comparatively thick coating with a value of 55.41 μm , as seen in Figure 2 (2). The coating exhibits a constant thickness of 61.4 μm for the HA + CaO composite layer, as shown in Figure 2. (3). The ultimate stacked combinations show higher thickness values, as shown in Figure 2 (4) and (5).

These samples have better qualities and a consistent covering. The thickness of the HA + (HA + CaO) + CaO layer (Figure 2 (4)) is 105.23 μm , whereas the CaO + (HA + CaO) + HA layer (Figure 2(5)) is 104.68 μm . The thickness measurements of the coating layers under optimal conditions, as seen by optical microscopy, are present-

Table 4. Lists the thickness of coating layers at optimal conditions in optical microscopy

No.	Type of sample	Thickness (μm) by optical
1	HA	21.23
2	CaO	55.41
3	Composite (HA + CaO)	61.4
4	(HA + Composite + CaO)	105.23
5	(CaO + Composite + HA)	104.68

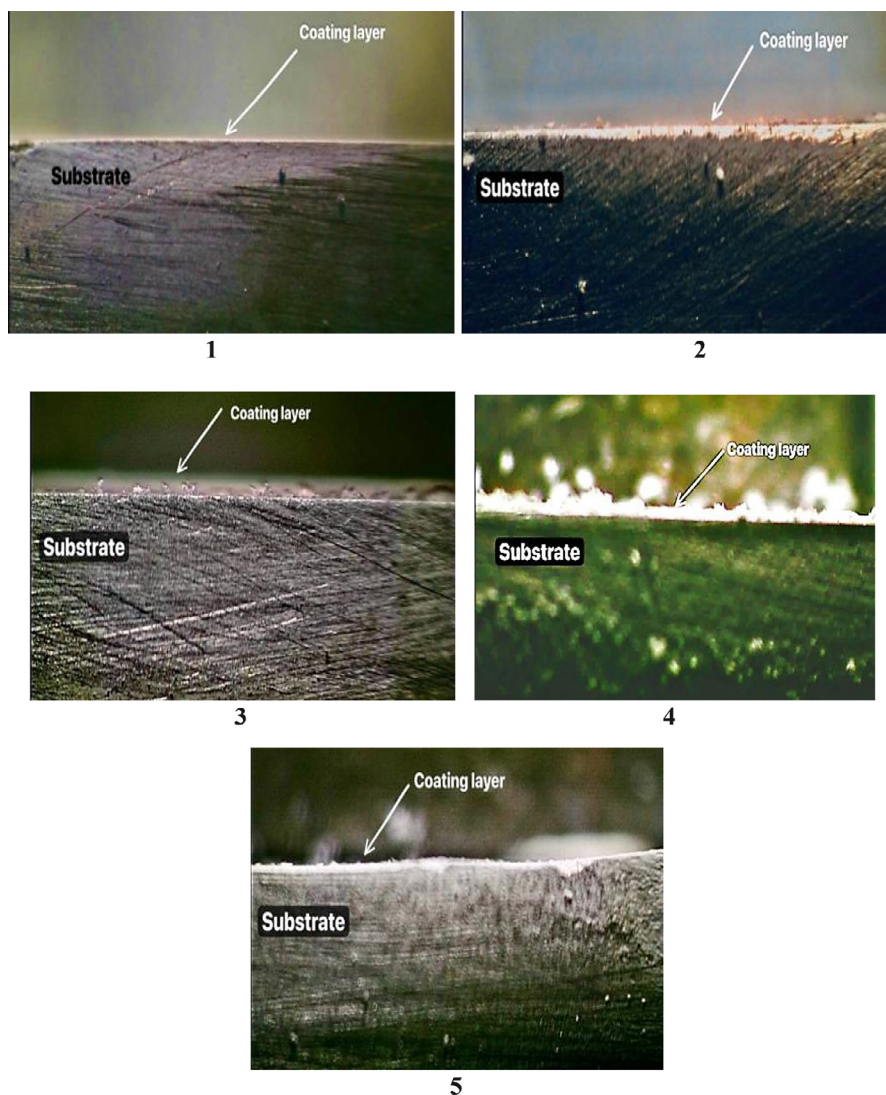


Figure 2. Optical images of cross section for coating samples. (1) one-layer HA, (2) one-layer CaO, (3) one-layer Composite (HA+CaO), (4) Three-layer (HA+ Composite +CaO) and (5) Three-layer (CaO+ Composite +HA)

ed in Table 4. The results of the optical microstructure measurements were verified using FESEM. According to the images, the coating was compact and uniform, showing a well-distributed structure and strong substrate adherence, indicating a steady and reliable deposition process as seen in Figure 3. A well-deposited, uniform coating covering the whole substrate surface is depicted in the FESEM cross-section photographs for the three-layer (HA + Composite + CaO) and (CaO + Composite + HA) in Figure 3(a) and (b),

with no fractures or gaps between the coating and the AZ31 substrate, suggesting a strong bond. Additionally, energy-dispersive X-ray spectroscopy (EDS) was performed to analyze the chemical composition of the coated AZ31 alloys, as illustrated in Table 5 and Table 6 for sample (4) HA + (HA + CaO) + CaO showed a high CaO content, while sample (5) CaO + (HA + CaO) + HA exhibited a higher HA concentration, enhancing bioactivity. The elemental distribution was homogeneous with strong adhesion to the substrate,

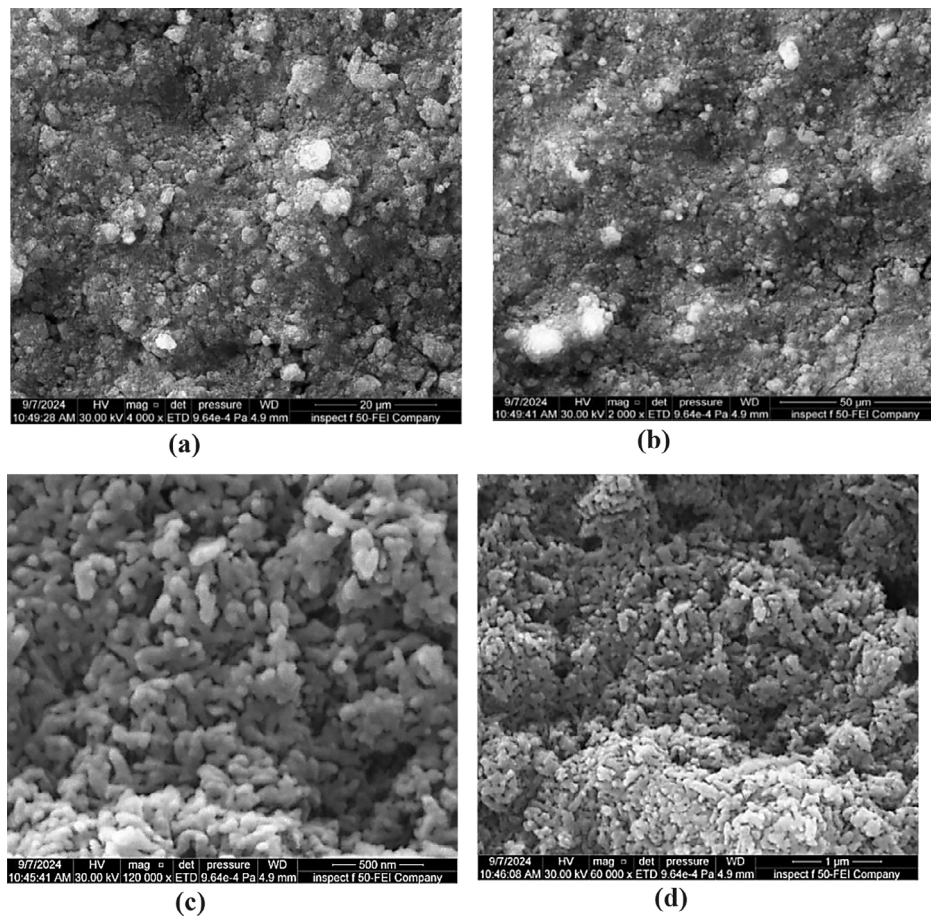


Figure 3. FESEM images of topography for coating samples (a) three-layer (HA+ Composite +CaO) and (b) three-layer (CaO + composite + HA) a3

Table 5. EDS for Three-layer (CaO + Composite + HA) coating sample

Element	Weight % error	Weight %	Atomic % error	Atomic %
C	0.2	20.8	0.4	35.2
O	0.7	33.4	0.8	42.4
Mg	0.1	1.0	0.1	0.8
Ca	0.2	39.6	0.1	20.1
Fe	0.1	1.0	0.1	0.4
Ni	0.1	1.1	0.0	0.4
Rb	0.5	3.1	0.1	0.7

Table 6. EDS for Three-layer (HA + Composite + CaO) coating sample

Element	Weight % error	Weight %	Atomic % error	Atomic %
C	0.5	26.5	0.9	43.1
O	1.4	27.0	1.7	33.0
Mg	0.1	0.6	0.1	0.4
Al	---	0.0	---	0.0
P	0.3	7.7	0.2	4.9
Ca	0.4	38.2	0.2	18.6

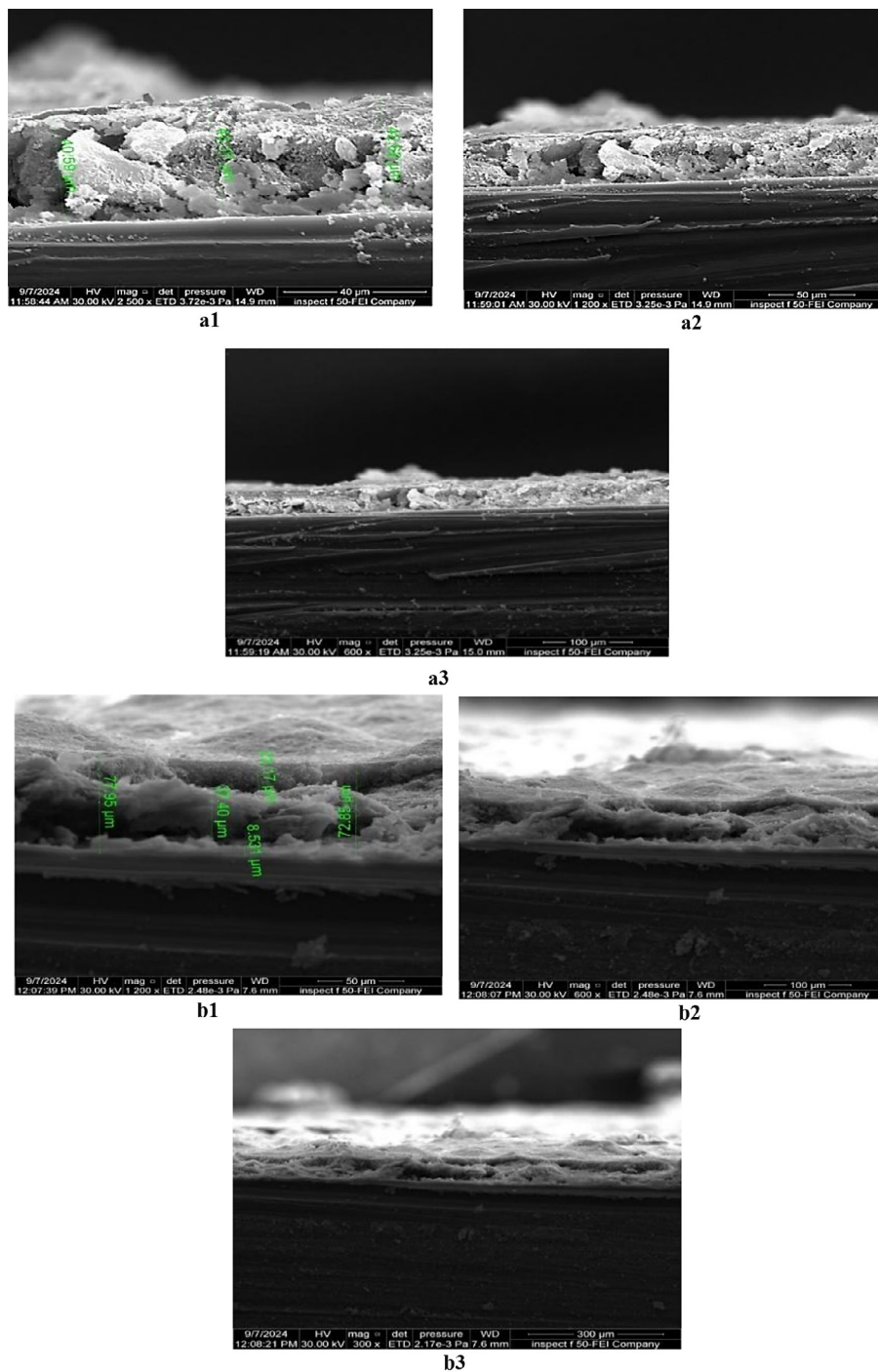


Figure 4. FESEM images of cross section for coating samples (a 1,2,3) Three layer (HA+ Composite + CaO) and (b 1,2,3) Three-layer (CaO+ composite + HA)

and the differences between the samples indicate the impact of layer arrangement on mechanical stability and bioactivity (Figure 4).

Wettability (contact angle)

Wettability is the ability of a chosen liquid to spread out and establish a close connection with a surface of interest. The most frequent method for determining wettability is to measure the angle of contact between a probe liquid and the surface. A hydrophilic surface has a high attraction for water molecules, which accelerates their spread and increases their interaction with the surface. A hydrophobic surface, on the other hand, minimizes interaction between water molecules and repels them, which results in the production of droplets. The angle at which the water molecules’ interface meets the biomaterial surface is known as the “contact angle” [4]. In general, the CA can vary from 0 to 180 degrees. Surfaces are classified as hydrophilic by water CAs below 90° and as super hydrophilic by CAs extremely near 0°. Hydrophobic surfaces are defined as having a water CA above 90°, while superhydrophobic surfaces have a CA above 150° [15].

Numerous studies have found that a hydrophilic surface significantly increases cell adhesion, spreading, proliferation, and differentiation. Another investigation indicated that osteoblast development occurs more readily on hydrophilic substrates (OH and NH₂ terminated self-assembled monolayers (SAMs)) than on hydrophobic substrates (COOH and CH₃ terminated SAMs) [16]. As a result, not only the coating’s adhesion to the substrate material but also the contact angle with deionized water were tested. A sessile drop of distilled water placed on a sample surface was used to evaluate the surface wetness. Table 7 depicts the contact angles with deionized water for different samples.

The surface wetting which was estimated by measuring the contact angles by a sessile drop of distilled water which was deposited on a sample surface. The contact angle of the uncoated AZ31sample is (60.958°), whereas the substrate with the coated with one-layer HA (17.996°), one-layer CaO (16.239°), one-layer of composite (HA + CaO (13.204°), the three-layer coating (HA + Composite + CaO) has a contact angle of 5.192°, and the three coating layers of (CaO+ Composite +HA) have the lowest angles (1.585°).

That means the composite (HA/CaO) has an important effect on adsorption and wetting behavior. The coating layer’s contact angle is displayed in Figure 5. When an implant material is placed inside the human body, one of the first critical interactions that occur is the wetting of the material by physiological fluids. This initial process plays a crucial role in controlling the subsequent adsorption of proteins onto the implant surface, which in turn influences cell attachment. Given this sequence of events, surface wettability is regarded as a key factor in determining the biocompatibility of an implant material [16]. In this work, an excellent stage of superhydrophilicity was achieved. The contact angle dropped to 1.5°, its lowest point.

The samples’ contact angles are listed in descending order: HA (17.996°) > CaO (16.239°) > Composite (HA + CaO) (13.204°) > (HA + Composite + CaO) (5.192°) > (CaO + Composite + HA) (1.585°).

Measurements of aluminum ion release

Proinflammatory cytokines are released when metal release is elevated. Furthermore, considerable amounts of aluminum ions released from the AZ31 Mg alloy may cause eczema, or allergic dermatitis [17]. To confirm that the AZ31 Mg alloy is suitable for use in the human body, the Aluminum Ion Release test is carried out. Parts per billion (ppb) and ppm were used to quantify the aluminum emission per sample surface. Table 8 shows the Al ion content released from the samples of Substrate, HA+(HA+CaO)+CaO, and CaO+HA+CaO)+HA after four weeks of immersion in a 0.9% NaCl solution as 0.00803 and 0.00133, respectively. The release of aluminum ions is more pronounced in the substrate, although it is slightly lower in the coated sample. Nevertheless, the coating sample is considered safe for human usage. The stability of the solution, the regularity and homogeneity of the coating layer,

Table 7. The measurement of contact angle for different samples

No.	Type of sample	Contact angle (°)
1	Substrate	60.985
2	HA	17.996
3	CaO	16.239
4	Composite (HA + CaO)	13.204
5	HA + comp. + CaO	5.192
6	CaO + comp. + HA	1.585

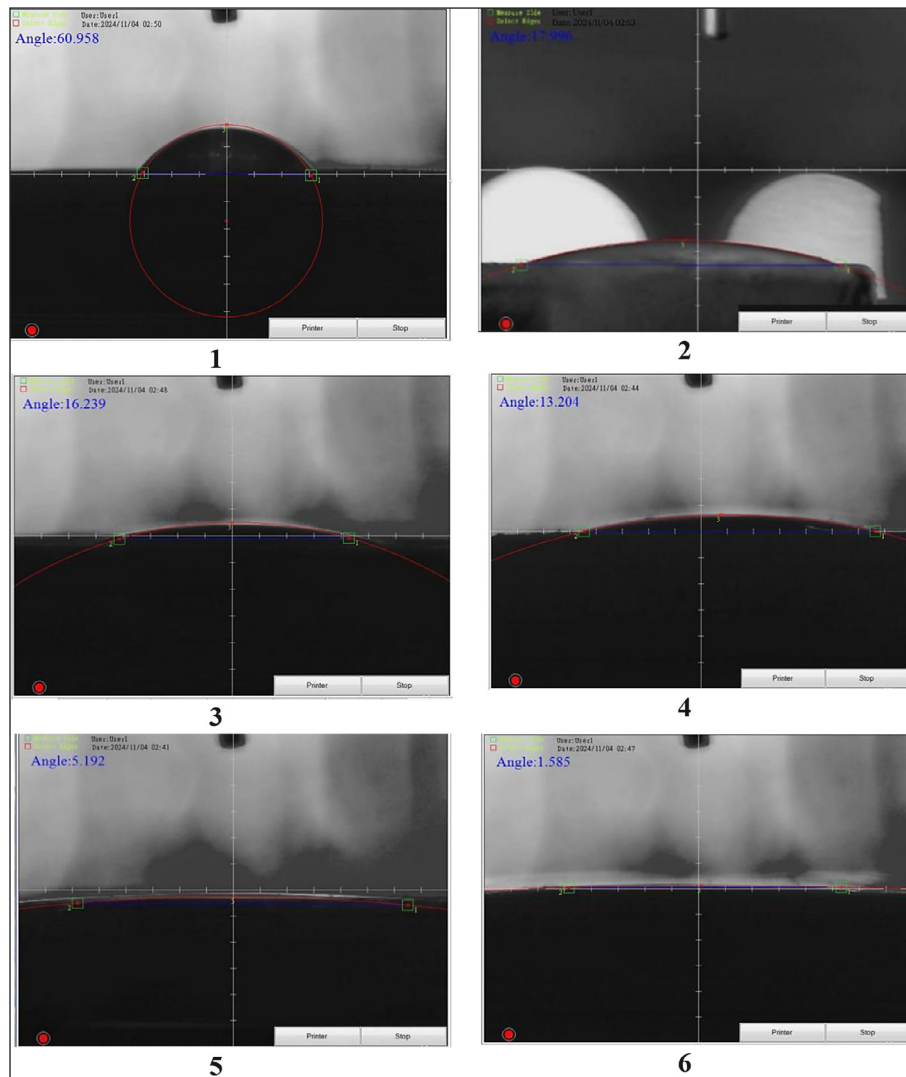


Figure 5. The contact angle of the coating layer test: (1) substrate (2) one layer HA (3) one layer CaO (4) one layer composite (5) three layer (HA+ composite +CaO) (6) Three layer (CaO + composite +HA)

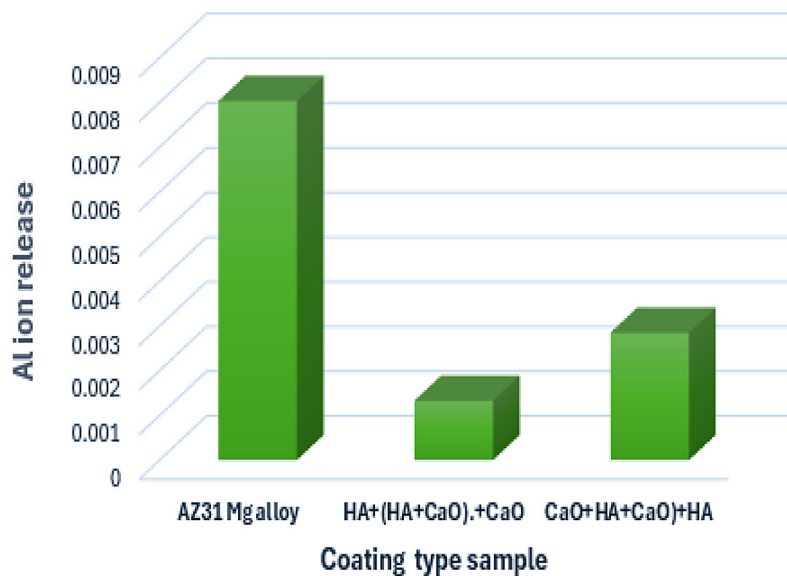


Figure 6. Shows the Al ion released in 0.9% NaCl for three samples at four weeks

Table 8. The Al ion released for three samples at four weeks

No.	Samples	Ion release for Al at four weeks (ppm)
1	AZ31 Mg Alloy	0.00803
2	HA + (HA + CaO) + CaO	0.00133
3	CaO + (HA + CaO) + HA	0.00285

and the absence of cracks are the causes of this phenomenon. After four weeks, the compound Al ion was released in samples in a 0.9% NaCl solution, as seen in Figure 6. When the investigated samples are exposed to 0.9% NaCl with either high or low porosity, the release of Al ions is exactly proportional to their porosity. It has a certain effect, especially when taking into account differences in the thickness and granular size of the coating. Through the formation of a physical and chemical barrier that inhibits Al oxidation and modifies its routes, these coatings prevent the release of Al ions into immersion solution [18].

Antibacterial assessment

Surface contamination on biomaterials poses a significant risk for microbial colonization, persistence, and subsequent infections. Since the primary application of this study is in the biomedical field, evaluating the antimicrobial properties of composite materials is crucial. Antimicrobial agents eliminate bacteria through various mechanisms, depending on the bacterial type. The Agar disk method was used to investigate the antibacterial inhibition zone, by measuring the inhibition zone formed around the samples. Two groups of the tested coating samples were used. Each group of samples was placed in a disk containing different type of bacteria. The first group was placed in a disk containing in *E. coli* bacteria, and the second group was placed in a disk containing in *Staph.* bacteria. The results of all coated samples

exhibited significant antibacterial activity against both *Escherichia coli* and *Staphylococcus aureus* during the incubation period, and the effect against *S. aureus* (gram-positive) was more than the effect against *E. coli* (gram-negative). In contrast, the uncoated magnesium AZ31 surface showed no inhibition of bacterial growth. Numerous bacterial colonies were observed on the uncoated areas after the test period, whereas the coated regions displayed substantial bacterial inhibition. The result of antibacterial activity against *E. coli* bacteria for samples (Three-layer (HA + Composite + CaO), Three-layer (CaO + Composite + HA), and uncoated magnesium substrate) were (38 mm, 29 mm, and 0 mm, respectively). The result of antibacterial activity against *Staphylococcus aureus* bacteria for the same samples were (46 mm, 40 mm, and 0 mm, respectively). Therefore, the presence of various concentrations of nanoparticles from (HA and CaO) inhibits bacterial growth. These materials are considered good antimicrobial agents due to their effective antibacterial properties. HA contributes to bacterial inhibition by promoting bioactivity, while CaO increases pH levels, creating an unfavorable environment for bacterial survival. They cause cell death and stop additional bacterial growth by damaging the membranes of the bacterium. Figure 7 and Figure 8 which also displays the antimicrobial coating inhibitory zone. Bacterial inhibition is indicated by the creation of a clear zone surrounding the disc. *Staphylococcus aureus* and *Escherichia coli*'s measured inhibitory zone for antimicrobial coating composition is displayed in Table 9.

Evaluation of bioactivity

The bioactivity of the coating is essential for enabling the proper integration of bone implants with living tissue. Thus, the test was applied on

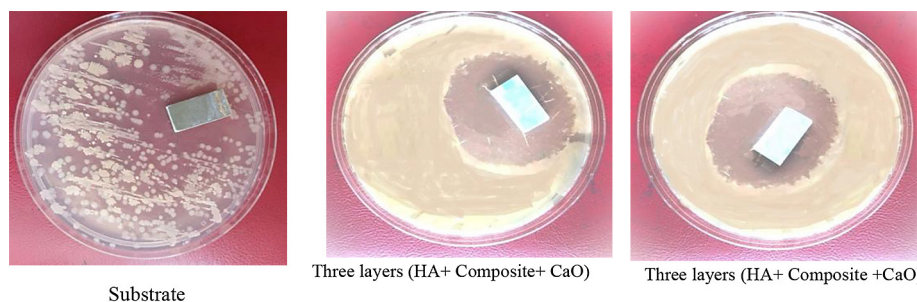


Figure 7. The images for (a) *Staph.* bacteria by Agar disk method

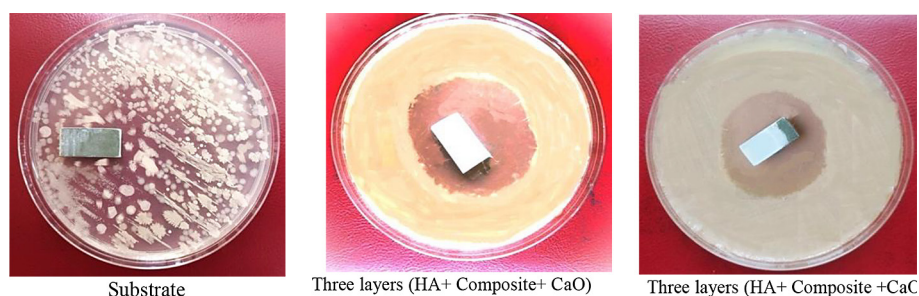


Figure 8. The images for (b) *E. coli* bacteria by Agar disk method

Table 9. Measured inhibition zone for antimicrobial coating composition of two types of bacteria *Staphylococcus aureus* and *E. coli*

No.	Type of sample	Zone of inhibition in Staph (mm)	Zone of inhibition in <i>E.coli</i> (mm)
1	Substrate	0	0
2	Three- layer (HA + Composite + CaO)	46	38
3	Three- layer (CaO + Composite + HA)	40	29

two samples: (HA + (HA + CaO) +CaO) and (CaO + (HA + CaO) + HA), which were specified via immersion in the SBF for evaluating their bioactivity. These samples were immersed in the SBF for two weeks. The bioactivity of the different coatings was analyzed using X-ray diffraction (XRD) and optical microscopy to study the layer

morphology and measure the change in thickness before and after immersion, which helped confirm the formation of the apatite layer. The results of the coating layer for three-layer (HA + Composite + CaO) and Three-layer (CaO + Composite + HA) before and after immersion in SBF are shown in Figure 9 and Figure 10 respectively.

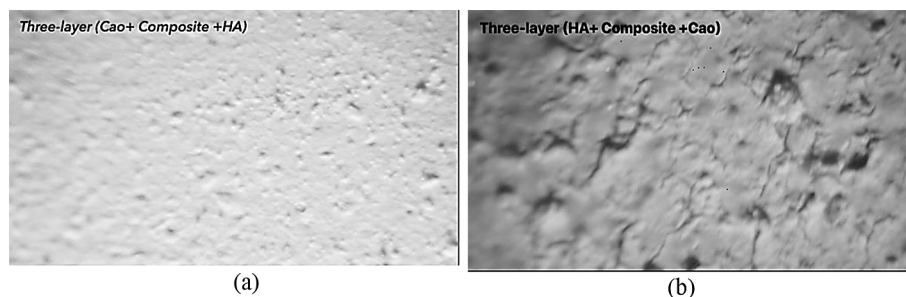


Figure 9. Optical microscopy images for three-layer (HA + Composite + CaO) (a) before immersion, (b) after 14 days immersion

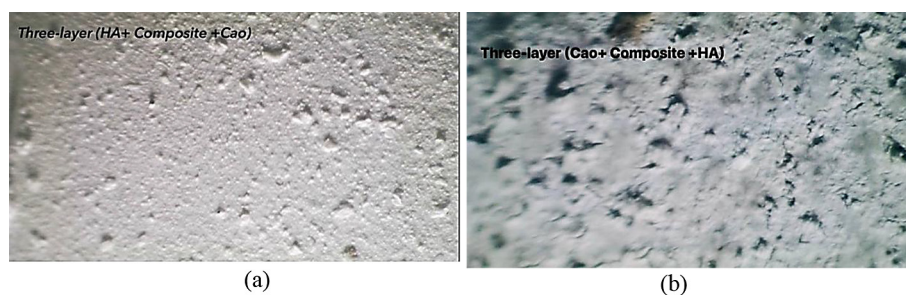


Figure 10. Optical microscopy images for three-layer (CaO + Composite +HA) (a) before immersion, (b) after 14 days immersion

The optical microscopy images revealed that the coated surfaces exhibited the formation of a hydroxyapatite (HA) layer after immersion, demonstrating the high bioactivity of these coatings. Furthermore, the results indicated that immersion for two weeks led to complete coverage of the surface with small and large hydroxyapatite particles, which appeared as clusters due to increased nucleation and growth of the mineralized layer, as shown in Figure 9 and Figure 10.

Thickness measurements using optical microscopy showed a noticeable increase after immersion for period of time, indicating the formation of the apatite layer on the coating surface. The thickness values recorded before and after immersion are presented in Table 10.

Additionally, cross-section images of the coatings, obtained using optical microscopy, are shown in Figure 11 and Figure 12, providing a detailed visualization of the thickness changes after immersion.

To further evaluate the phase composition and validate the development of apatite both before and after immersion, XRD characterization was performed after the optical microscope investigation. Prior to immersion, the XRD pattern of the (HA + Composite + CaO) coating (Figure 13a) showed distinct diffraction peaks at $2\theta = 37.360^\circ$ (200), 32.052° , 32.196° (111), 53.852° (220), 49.494° , and 51.592° . The most intense peak appeared at $2\theta = 37.360^\circ$ (200), which corresponds to CaO, indicating its dominance in the outer layer of this multilayer structure. The co-presence of HA and CaO peaks confirmed successful deposition of the three layers with full surface coverage, as no substrate signals were detected. Meanwhile, the XRD pattern of the (CaO + Composite + HA) coating (Figure 14a) exhibited major peaks at $2\theta = 32.052^\circ$, 32.196° (111), 37.360° (200), 53.852° (220), 25.879° , and 34.060° . The dominant peak at $2\theta = 32.052^\circ$ corresponds to HA, indicating a well-structured multilayer coating with no visible magnesium

Table 10. Thickness values of coatings before and after immersion in SBF

No	Type of sample	Thickness before immersion (μm)	Thickness after immersion (μm)
4	(HA + Composite + CaO)	105.23	164
5	(CaO + Composite + HA)	104.68	146.85

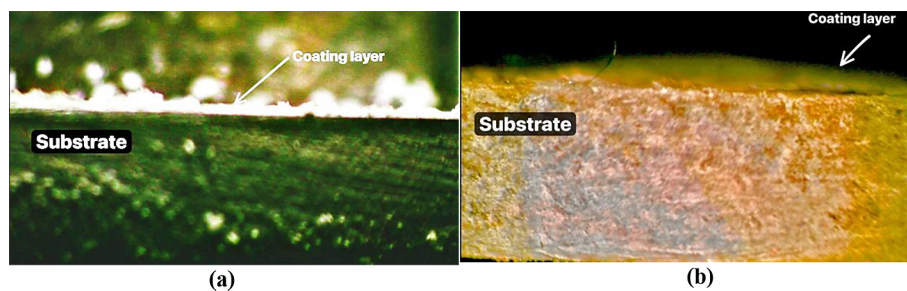


Figure 11. Optical microscopy images of cross section for three-layer (HA + Composite + CaO) (a) before immersion, (b) after 14 days immersion

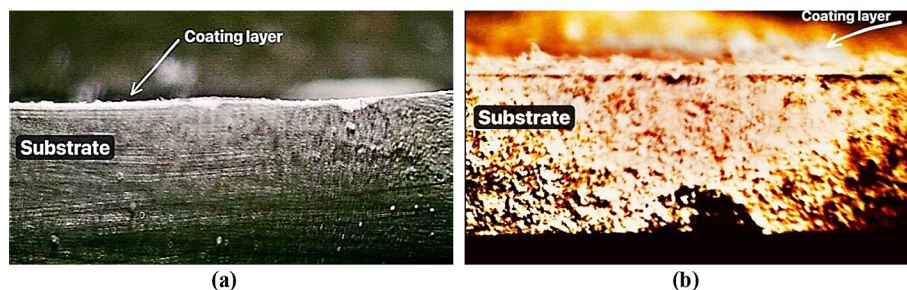


Figure 12. Optical microscopy images of cross section for three-layer (CaO + Composite + HA) (a) before immersion, (b) after 14 days immersion

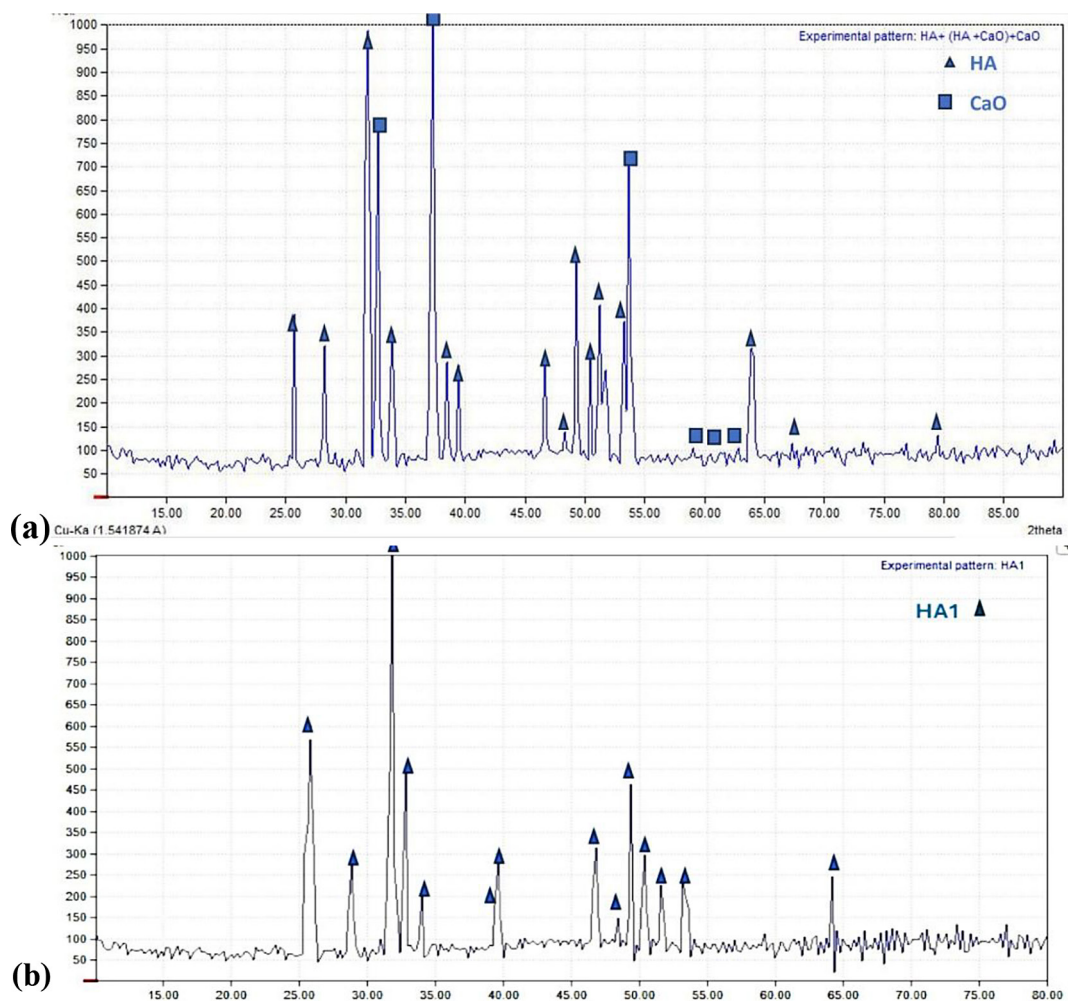


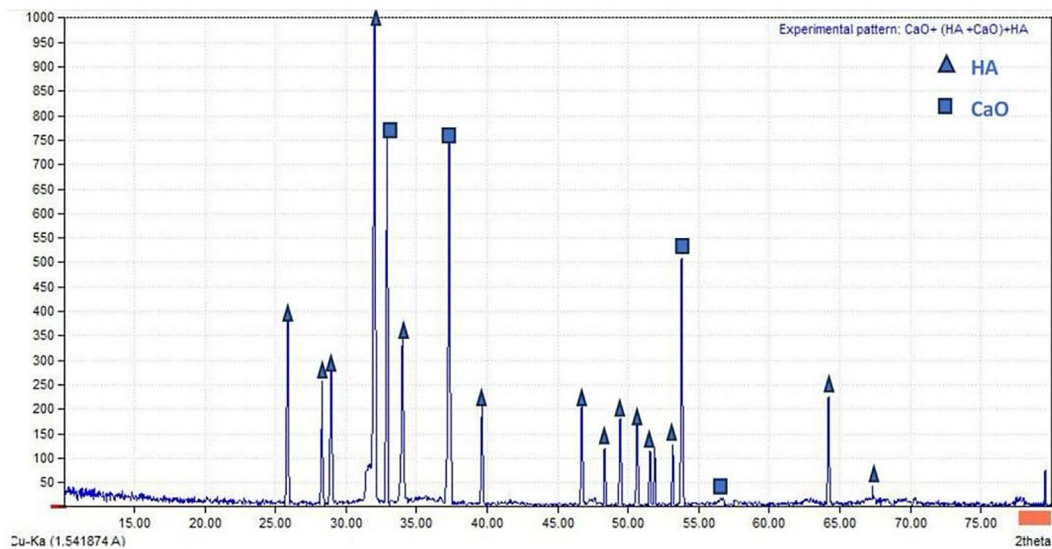
Figure 13. XRD pattern of (a) three-layer coating (HA + Composite + CaO) before immersion in SBF and (b) after two weeks of immersion in SBF

substrate peaks. After two weeks of immersion in SBF, significant changes were observed in the XRD patterns, highlighting the transformation and bioactivity of the coatings. For the (HA + Composite + CaO) coating, the post-immersion XRD pattern (Figure 13b) revealed characteristic diffraction peaks at $2\theta = 31.773^\circ$ (211), 25.879° (002), 32.902° (300), and 49.468° (213). The most intense peak was located at $2\theta = 31.773^\circ$ (211), which corresponds to hydroxyapatite (HA), according to JCPDS card No. 09-0432. The absence of CaO or magnesium substrate peaks shows that CaO was completely transformed into HA via ion exchange with the surrounding fluid, emphasizing the structure's bioactive properties. Similarly, the XRD pattern of the (CaO + Composite + HA) coating after immersion (Figure 14b) displayed prominent HA-related peaks at $2\theta = 31.773^\circ$ (211), 32.902° (300), 25.879° (002), and 49.468° (213), with the most intense peak also found at $2\theta = 31.773^\circ$

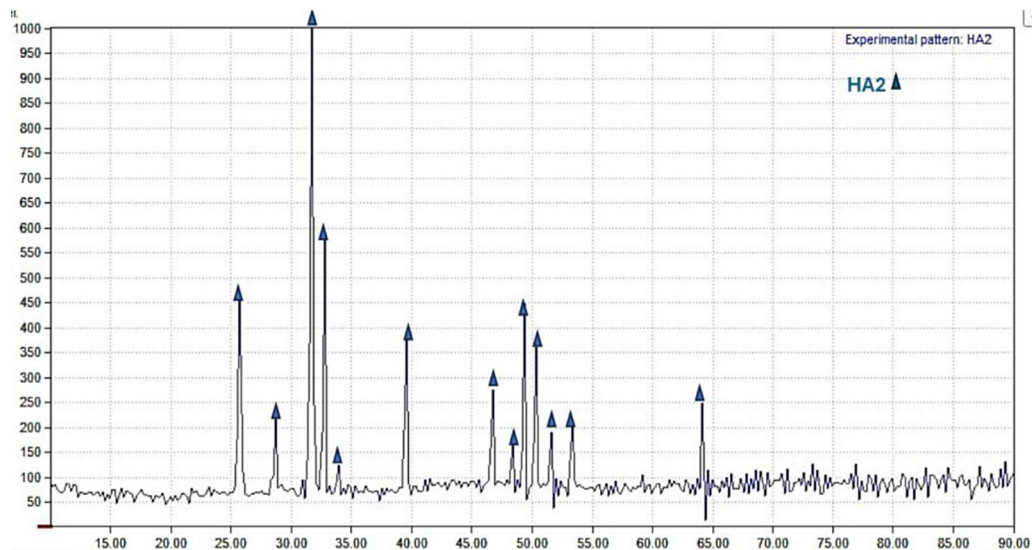
(211). These results indicate the successful formation of HA on both coated surfaces. Interestingly, no peaks associated with the magnesium substrate nor CaO were seen, indicating complete surface coverage and potential ionic exchange-induced conversion of CaO to HA in the SBF. This demonstrates the bioactive nature of both multilayer coatings and their ability to promote apatite nucleation and development, which is essential for improving osseointegration in biomedical applications. These XRD data highlight the potential of both multilayer coatings to improve bone integration in biomedical implant applications by offering compelling proof of their bioactivity when combined with the optical microscopy results.

Corrosion behavior of the coating

A cyclic polarization test was performed for all samples in simulated body fluid (SBF)



(a)



(b)

Figure 14. XRD pattern of (a) three-layer coating (CaO + Composite + HA) before immersion in SBF and (b) after two weeks of immersion in SBF

solution to evaluate their corrosion resistance performance. The polarization curves were recorded as shown in Figure 15, while the values of corrosion potential (E_{corr}) and corrosion current density (I_{corr}) were extracted using the Tafel extrapolation method. The results are summarized in Table 11. The results indicate that the uncoated surface exhibited the highest susceptibility to corrosion, recording a very low corrosion potential value of -1442.83 mV and a high corrosion current density (0.198496 μA), indicating low corrosion resistance in this case. Similarly, the single-layer HA coating did not show significant improvement in corrosion behavior, as its measured values were quite

similar to those of the uncoated surface. In contrast, samples coated with a single layer of CaO or a composite layer (HA + CaO) demonstrated a noticeable enhancement in corrosion resistance, as reflected by a clear reduction in corrosion current density and a relative improvement in corrosion potential values. This suggests that these coatings provided better protection for the substrate. The best performance was observed in the samples with triple-layer coatings, particularly the sample with the sequence (CaO + (HA + CaO) + HA), which exhibited the highest corrosion resistance by achieving the lowest corrosion current density (0.0619633 μA) and the highest corrosion potential among

Table 11. Results of electrochemical corrosion parameters following corrosion testing on all Layers upon immersion in SBF

No.	Type of sample	Current [μ A]	Potential [mV]
1	Without coating	0.198496	-1442.83
2	HA	0.198496	-1326.55
3	CaO	0.181312	-1273.26
4	HA + CaO	0.0901688	-1200.58
5	HA(HA+CaO) + CaO	0.0733109	-1016.47
6	CaO+(HA+CaO) + HA	0.0619633	-895.349

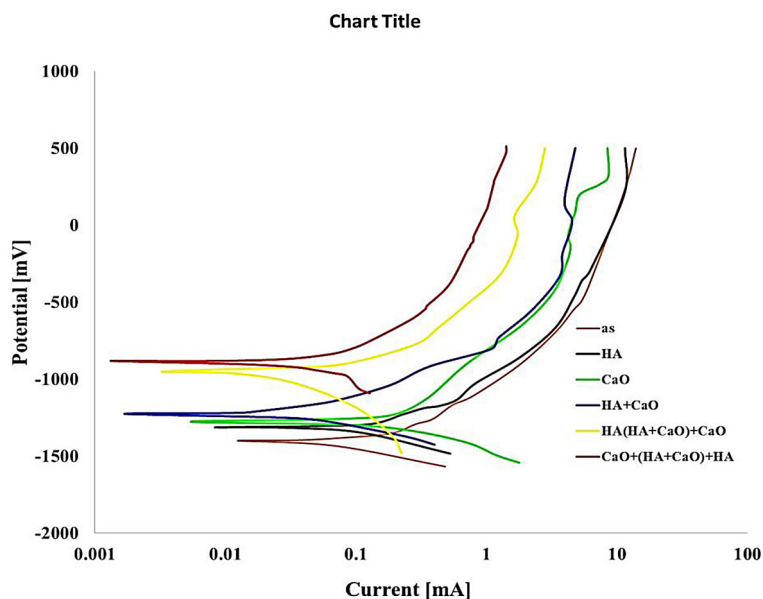


Figure 15. Cyclic polarization curves of (1) substrate (2) one layer HA (3) one layer CaO(4) one layer composite (5) Three layer (HA+ composite +CaO) (6) Three layer (CaO + composite +HA)

all samples (-895.349 mV). This indicates the formation of an effective protective layer that prevents the corrosive medium from reaching the metallic surface. Based on these results, the corrosion resistance of the samples can be ranked in descending order (from the best to the worst) as follows: CaO+(HA+CaO) +HA > HA+(HA+CaO) +CaO > HA+CaO > CaO > HA > Uncoated surface

CONCLUSIONS

CaO and HA composite coatings were successfully applied to AZ31 magnesium alloy using EPD. Zeta potential measurements confirmed the stability of the coating suspensions, ensuring uniform deposition across the substrate. Microstructural analyses using SEM and optical

microscopy revealed that the coatings were uniform, free of cracks, and exhibited strong adhesion to the substrate. Wettability tests showed that the coated samples exhibited super hydrophilic properties, which enhance bioactivity and cell adhesion.

Antibacterial testing demonstrated that the HA/CaO composite coatings significantly inhibited bacterial growth, particularly against *Staphylococcus aureus*, thereby reducing the risk of post-implant infections. Bioactivity assessments in SBF indicated the formation of an appetite layer, confirming the coatings' potential to support bone integration. These results suggest that HA/CaO coatings substantially improve the corrosion resistance, antibacterial efficacy, and osteoconductivity of AZ31 magnesium alloy, highlighting its promise as a biodegradable material for orthopedic implants.

REFERENCES

- Chong, E.T.J., Ng, J.W. and Lee, P.-C. Classification and medical applications of biomaterials—a mini review. *BIO integration* 2023; 4(2): 54. <https://doi.org/10.15212/bioi-2022-0009>
- Oleksy, M., Dynarowicz, K., Aebisher, D. Advances in biodegradable polymers and biomaterials for medical applications – A review. *Molecules*, 2023; 28(17): 6213. <https://doi.org/10.3390/molecules28176213>
- Velu, R., Calais, T., Jayakumar, A., Raspall, F.A comprehensive review on bio-nanomaterials for medical implants and feasibility studies on fabrication of such implants by additive manufacturing technique. *Materials*, 2020; 13(1): 92. <https://doi.org/10.3390/ma13010092>
- Davis, R., Singh, A., Jackson, M.J., Coelho, R.T., Prakash, D., Charalambous, C.P., Ahmed, W., da Silva, L.R.R., and Lawrence, A.A. A comprehensive review on metallic implant biomaterials and their subtractive manufacturing. *The International Journal of Advanced Manufacturing Technology* 2022; 120(3): 1473–1530. <https://doi.org/10.1007/s00170-022-09088-8>
- Rahman, M., Li, Y., and Wen, C. HA coating on Mg alloys for biomedical applications: A review. *Journal of Magnesium and Alloys* 2020; 8(3): 929–943. <https://doi.org/10.1016/j.jma.2020.05.009>
- Zhang, T., Wang, W., Liu, J., Wang, L., Tang, Y., Wang, K. A review on magnesium alloys for biomedical applications. *Frontiers in Bioengineering and Biotechnology*, 2022; 10: 953344. <https://doi.org/10.3389/fbioe.2022.953344>
- Gao, J., Su, Y., and Qin, Y.-X. Calcium phosphate coatings enhance biocompatibility and degradation resistance of magnesium alloy: Correlating in vitro and in vivo studies. *Bioactive Materials* 2021; 6(5): 1223–1229. <https://doi.org/10.1016/j.bioactmat.2020.10.024>
- Al-Ghuraibawi, A., Abed, A.H., Mansor, K.K. Simulation and experimental approach for metal forming with a multi-point die. *Salud, Ciencia y Tecnologia - Serie de Conferencias*, March 2024; 36. <https://doi.org/10.56294/sctconf2024855>
- Mohammed, H.K., Abbas, A.S. and Mustafa, A.M. Characteristics and properties of bright nickel plated on aluminum substrate type AA-1100. In *AIP Conference Proceedings*, AIP Publishing, 2024; 3002(1). <https://doi.org/10.1063/5.0206370>
- Khelifi, K., Dhiflaoui, H., Ben Rhouma, A., Faure, J., Benhayoune, H., Ben Cheikh Laarbi, A. Nano-mechanical behavior, adhesion and corrosion resistance of hydroxyapatite coatings for orthopedic implant applications. *Coatings*, 2021; 11(4): 477. <https://doi.org/10.3390/coatings11040477>
- Omarov, S., Nauryz, N., Talamona, D., Perveen, A. Surface modification techniques for metallic biomedical alloys: A concise review. *Metals*, 2023; 13(1): 82. <https://doi.org/10.3390/met13010082>
- Levengood, S.L., Zhang, M. Chitosan-based scaffolds for bone tissue engineering. *Journal of Materials Chemistry B: Materials for Biology and Medicine*, 2014; 2(21): 3161–3184. <https://doi.org/10.1039/C4TB00027G>
- Jasim, A.N., Mohammed, A., Mustafa, A.M., Sayyid, F.F., Aljibori, H.S., Al-Azzawi, W.K., Al-Amiery, A.A. and Yousif, E.A. Corrosion inhibition of mild steel in HCl solution by 2-acetylpyrazine: weight loss and DFT studies on immersion time and temperature effects. *Progress in Color, Colorants and Coatings* 2024; 17(4): 333–350. <https://doi.org/10.30509/pccc.2024.167231.1261>
- Saji, V.S. Electrophoretic (EPD) coatings for magnesium alloys. *Journal of Industrial and Engineering Chemistry* 2021; 103: 358–372. <https://doi.org/10.1016/j.jiec.2021.08.002>
- Hamood, A.F., Habeeb, H.M., Abdulhussein, B.A., Mustafa, A.M., Sayyid, F.F., Hanoon, M.M., Gaaz, T.S., Hameed, L.A., and Alamiery, A.A.A. Weight loss, electrochemical measurements and DFT studies on corrosion inhibition by 7-mercapto-4-methylcoumarin. *Results in Engineering* 2024; 23: 102677. <https://doi.org/10.1016/j.rineng.2024.102677>
- Hubbe, M.A., and Gardner, D.J. Contact angles and wettability of cellulosic surfaces: a review of proposed mechanisms and test strategies. *Bio-Resources* 2015; 10(4). https://doi.org/10.15376/biores.10.4.Hubbe_Gardner_Shen
- Gittens, R.A., Scheideler, L., Rupp, F., Hyzy, S. L., Geis-Gerstorfer, J., Schwartz, Z., and Boyan, D.B. A review on the wettability of dental implant surfaces II: Biological and clinical aspects. *Acta biomaterialia* 2014; 10(7): 2907–2918. <https://doi.org/10.1016/j.actbio.2014.03.032>
- Nouri, A., and Cuie Wen. Introduction to surface coating and modification for metallic biomaterials.” *Surface coating and modification of metallic biomaterials* 2015; 3–60. <https://doi.org/10.1016/B978-1-78242-303-4.00001-6>
- Mahajan, A., and Sidhu, S.S. Surface modification of metallic biomaterials for enhanced functionality: a review. *Materials technology* 2018; 33(2): 93–105. <https://doi.org/10.1080/10667857.2017.1377971>
- Hussein, M.B., Abdulkareem, M.H., Mustafa, A.M. A study evaluating the improvement of the corrosion properties of a Ytria-stabilized zirconia coated on Ti-alloy by using a Taguchi design. *AIP Conf Proc.* 2024; 3229(1). <https://doi.org/10.1063/5.0236016>
- Hussein, M.B., Mustafa, A.M., Abdulkareem, M.H., and Alamiery, A. Comparative corrosion performance of YSZ-coated Ti-13Zr-13Nb alloy and commercially

- pure titanium in orthopedic implants. *South African Journal of Chemical Engineering* 2024; 48(1): 40–54. <https://doi.org/10.1016/j.sajce.2024.01.005>
22. Hussein, M.B., Mustafa, A.M., and Abdulkareem, M.H. A Comparative study on dip coating and corrosion behavior of Ti-13Zr-13Nb and commercially pure titanium alloys coated with YSZ by Taguchi design. *Salud, Ciencia y Tecnología-Serie de Conferencias* 2024; 3: 847. <https://doi.org/10.56294/sctconf2024847>
23. Abd Muslim, H.W., Mundher, M.A., Farhan, S.F. Corrosion Inhibition Performance of Whey Protein-Derived Inhibitors for Low Carbon and Dead Mild Steels in 1M Hydrochloric Acid. *Salud, Ciencia y Tecnología - Serie de Conferencias*. 2024; 3: 849. <https://doi.org/10.56294/sctconf2024849>
24. Abass, M.H., Abdulkareem, M.H., and Hussein, H.A. Effect of annealing treatment on (Mg17Al12) phase characterization and corrosion behavior in different solutions for AZ91 alloy. *Advances in Science and Technology. Research Journal* 2023; 17(2). <https://doi.org/10.12913/22998624/161831>
25. Taha Mohamed, M., Nawawi, S.A., Mustafa, A.M., Sayyid, F.F., Hanoon, M.M., Al-Amiery, A.A., Kadhum, A.A.H., and Al-Azzawi, W.K. Revolutionizing corrosion defense: unlocking the power of expired BCAA. *Progress in Color, Colorants and Coatings* 2024; 17(2): 97–111. <https://doi.org/10.30509/pccc.2023.167156.1228>
26. Abdulhasan, A.A., Sheng, E.L., Mustafa, A.M. and Isa, M.R.B. Recent advancements in biocompatible coatings for metallic and non-metallic biomaterials: A review. *Corrosion Science and Technology* 2024; 23(5): 449–469. <https://doi.org/10.14773/CST.2024.23.5.449>
27. Abbas, A.S., Mahdi, B.S., Abbas, H.H., Sayyid, F.F., Mustafa, A.M., Annon, I.A., Abdulsahib, Y.M., Resen, A.M., Hanoon, M.M., and Obaeed, N.H. Corrosion behavior optimization by nanocoating layer for low carbon steel in acid and salt media, *Corrosion Science and Technology* 2023; 22(1). <https://doi.org/10.14773/cst.2023.22.1.1>
28. Mohamed, M.T., Nawawi, S.A., Algailani, H.M., Al-rubaiy, A.A.A.G., Mahmoud, A.K., Farman, S., Mustafa, A.M., and Alamiery, A.A. Evaluation of the mechanical performance of iron–polymethyl methacrylate and polystyrene polymer products based on alumina nanomaterials. *Advances in Science and Technology Research Journal* 2025; 19(3): 202–210. <https://doi.org/10.12913/22998624/199471>
29. Abdulridha, H.H., Abbas, T.F., and Bedan, A.S. Investigate the effect of chemical post processing on the surface roughness of fused deposition modeling printed parts *Advances in Science and Technology Research Journal*, 2024; 18(2): 47–60. <https://doi.org/10.12913/22998624/183528>
30. Abed, A.K., Mustafa, A.M., and Resen, A.M. Assessment corrosion and bioactive behavior of bio-glass coating on Co-Cr-Mo alloy by electrophoretic deposition for biomedical applications, *Corrosion Science and Technology* 2024; 23: 179. <https://doi.org/10.14773/cst.2024.23.3.179>